Polymer 55 (2014) 6390–6398

Contents lists available at ScienceDirect

Polymer

journal homepage: www.elsevier.com/locate/polymer

Control of the electric field–polymer solution interaction by utilizing ultra-conductive fluids

N.M. Thoppey [a], R.E. Gorga [a], L.I. Clarke [b, **], J.R. Bochinski [b, *]

[a] Fiber and Polymer Science Program, NC State University, Raleigh, NC 27695, USA
[b] Department of Physics, NC State University, Raleigh, NC 27695, USA

ARTICLE INFO

Article history:
Received 5 September 2014
Received in revised form
3 October 2014
Accepted 4 October 2014
Available online 12 October 2014

Keywords:
Unconfined electrospinning
Electric field interactions
Nanofibers

ABSTRACT

Dramatically raising the conductivity of a polymer solution by using a salt additive allows control over the electric field-induced jet feed rate when electrospinning from an unconfined fluid without altering the applied voltage. As the solution conductivity increases, the flow rate drops by an order of magnitude. At a high voltage level and fluid conductivity value, the jets undergo a whipping instability over almost the entire path from the source to the collector experiencing only a negligibly short linear region which, along with the flow rate data, indicates that the jet narrows due to the high conductivity. Under these conditions, even while possessing relatively large individual jet feed rates, thin diameter nanofibers (200–300 nm) are readily produced. In contrast with other approaches to obtain narrow fibers from unconfined fluids (e.g., voltage reduction to control feed rate), here the fiber forming jets are present indefinitely. Continuous, scaled up nanofiber production rate of >125× over the traditional single needle electrospinning method is observed from the presence of multiple jets, each possessing a relatively high solution feed rate. These fundamental experiments reveal new pathways for exploring novel electrospinning configurations where the jet feed rate can be controlled by manipulating the solution conductivity.

© 2014 Elsevier Ltd. All rights reserved.

1. Introduction

Nanofibrous materials have utility in wide-ranging applications including sensors [1–4], biomechanical scaffolds for tissue regeneration [5–8] and controlled chemical-release [9–11], as high-efficiency filtration media [12,13], and for efficacious energy conversion and storage [14–18]. Polymeric nanofibers are particularly important due to the ease of forming fibers from a wide range of materials, including varying compositions and additives, and low cost. Such useful nanomaterial is comprised of collections of individual fibers having sub-micron diameters and high surface-to-volume ratios with randomly-oriented fiber ensembles possessing an intrinsically large porosity value (~70%) [19].

While alternative production methods have been regularly proposed [20,21], traditional solution-phase needle electrospinning [22] (TNE) remains the most commonly utilized research scale technique to generate polymeric nanofibers. In this approach, a polymer solution is expelled through an enclosed aperture using a precisely-dispensing mechanical pump while subjected to an electric field. The resultant polymer fluid jet (where ideally the pump rate and the rate of removal by electrostatic forces matches) moves in a linear path while reducing its diameter before undergoing a charge-driven, bending (or whipping) instability and finally depositing as a dried nanofiber onto the electrically-grounded collector. The well-formed fibers are randomly-oriented and nanoscale in diameter (e.g. ~200 nm). Other more complex forms of TNE such as coaxial electrospinning [23,24] for creating bi-component fibers, and newer [25–29] approaches for improved single-component fibers have also been demonstrated.

Although an optimized TNE process produces high quality nanofibers (i.e., fibers with small diameters and a narrow distribution of diameter sizes), the fabrication process is slow [19,30,31] (e.g., 0.01–0.1 g/hr), which presents a practical limitation for industrial-level utilization of these materials. Increased nanofiber production rate has been demonstrated by concurrently utilizing several needles [32–37], spinnerets with multiple nozzles [38], or analogous structures having many apertures [30,31,39], but such methods are often complicated to implement and prone to

* Corresponding author.
** Corresponding author.
E-mail addresses: laura_clarke@ncsu.edu (L.I. Clarke), jason_bochinski@ncsu.edu (J.R. Bochinski).

http://dx.doi.org/10.1016/j.polymer.2014.10.007
0032-3861/© 2014 Elsevier Ltd. All rights reserved.

clogging. To avoid these detriments, alternative scale-up electrospinning methods which utilize polymer fluid in an unconfined manner [40] (i.e., spinning directly from a reservoir or sheet of fluid without a confining orifice) have been developed, including needleless electrospinning [41], cleft electrospinning [42], roller electrospinning [43–45] (and analogous geometries [46,47]) using a fluid bath, free surface electrospinning [48], as well as the recently demonstrated edge electrospinning, which is utilized in this work [49–52]. As reported previously [49–53] under unconfined electrospinning and utilized in this work, stationary fluid is subjected to a strong electric field and deforms, creating fingering perturbations which eventually transition into cone-jets (with fluid being expelled from the cone terminus). The average spacing between the fiber-forming cone-jets is set by either interaction between the surface tension and field or inter-jet interactions. The flow through each jet is determined by the fluid properties and the applied electric field.

Successful electrospinning for the production of well-formed nanofibers requires the polymer fluid to possess key properties within a nominal range (namely, certain values of viscosity, surface tension, and conductivity [54–56]). Tuning fluid properties may be particularly important in an unconfined environment because the system is innately less constrained; for instance, fluid flow is not explicitly, independently controlled. Overfeeding is a common problem in unconfined geometries resulting in larger than optimal fiber diameter or insufficient solvent loss and thus damage to the fibrous mat. In this report, we focus specifically on the effect of solution conductivity in an unconfined electrospinning geometry where fluid is directly in contact with a charged metal object (in this case, a metal reservoir with a sharp lip), jets form spontaneously on the fluid surface, and jet formation and fluid flow through each jet is solely controlled by the interactions between the fluid and electric field (i.e., no mechanical or gravity driven pumping is present). Due to low cost and chemical compatibility, inorganic salts have been widely utilized as dopants in polymer solutions to improve the electrospinning process via alteration of conductivity. The impact of different salts on the conductivity varies depending upon ionic size, ionic mobility, and concentration of the additive compound. Numerous research studies have empirically explored the efficacy of adding a low quantity of salt (i.e., commonly <<1 weight percent (wt %)) to the spinning solution, and reported the effect on the nanofiber morphology [41,55,57–82]. Under many processing conditions, salt addition results in fabrication of better-formed (e.g., the elimination of beads) and narrower diameter fibers [56,81,83]. (Nanofibers commonly possess smooth morphology while a few experiments have intentionally created porous fibrous structures [84,85].) When higher salt levels are used (>1 wt %), it is often reported that the TNE process is unstable [80] or not achievable [81,86]. We note that most previous studies change the solution conductivity while keeping all other experimental parameters constant, in particular keeping the applied voltage relatively small, as is needed for a moderate conductivity solution.

As mentioned above, the optimal applied voltage required to form or maintain cone-jets in an unconfined geometry often results in very high feed rates for low or moderate conductivity solutions, which are inconsistent with high-quality fiber formation; in order to develop high quality, high throughput electrospinning strategies both jet formation and control of jet flow rate must be simultaneously optimized. Too strong of a field–fluid interaction results in jet overfeeding and delivery of wet solution directly to the collector, a detrimental process referred to as “streaming”, whereas if the applied voltage is too small it cannot sustain the instabilities and jet extinction results. Various strategies [50–52] have been developed to address this counter-balance between jet stability and high-quality fiber formation, namely the use of different voltage levels to initiate and then maintain jets (i.e., the use of the hysteretic regime). Here we explore an alternative approach: tuning of solution conductivity to decrease flow rate without impacting jet stability, enabling formation of a high volume of high quality fibers. Only a few reports have previously discussed the potential benefits of increased solution conductivity in unconfined scaled-up electrospinning systems [43,44], working within the moderate conductivity range with a focus on fiber diameter.

In the present report, increasing the solution conductivity into a regime where electrospinning is normally not achieved provides new insights into the dynamics of the electrospinning process and more broadly the interaction between strong electric fields and polymer solutions. We observe that electrospinning is possible for ultrahigh conductivity (30 mS/cm) solutions at a high applied voltage and that flow rate decreases exponentially with conductivity in the moderate (~100 μS/cm) to high conductivity regime. Spontaneously formed jets are permanently present (as demonstrated by electrospinning for several hours with a continuously replenished polymer solution reservoir) and the resultant fibers have similar diameter (193 ± 25 nm) to those produced from moderate conductivity solutions of the same polymer electrospun under optimal conditions in a traditional needle approach (262 ± 19 nm) [50]. We argue that the decrease in jet diameter and increase in surface charge density as solution conductivity increases results in enhancement of the whipping regime. The very long whipping region (beginning almost immediately at the bowl edge) enables narrow fibers to be formed at relatively high feed rates. Although here enhanced conductivity is achieved via a simple salt (NaCl), this approach could also be usefully utilized by analogous means; e.g., with a transient compound to provide additional ions during the fabrication process [75] which could be neutralized in the final solid fiber.

2. Experimental methods

2.1. Materials

The semi-crystalline polymer polyethylene oxide (PEO) having an average molecular weight of 400,000 g/mol (Scientific Polymer Products) was used without further purification in all experiments and de-ionized water (H_2O) having a resistivity of 18 MΩ was utilized as the solvent. Additionally, a trace amount of Rhodamine 590 Chloride (R6G, 05901, 479 g/mol) (Exciton) (0.001 wt %) was added to enhance viewing contrast when imaging the electrospinning process. To controllably vary solution conductivity, differing amounts (0–1.96 wt %) of the inorganic salt sodium chloride (NaCl, crystalline/certified ACS) (Fisher Scientific) was mixed into ~4 wt % PEO solutions and stirred at room temperature for 24 h to ensure complete dissolution. Table 1 lists the different solution

Table 1
Composition of solutions #1–7, ~4 wt % polymer with varying concentrations of salt.

Solution #	Components (g)				Concentration (wt %)	
	PEO	NaCl	R6G	H_2O	Polymer	Salt
1	4	0	0.001	96	4.00	0
2	4	0.01	0.001	96	4.00	0.01
3	4	0.05	0.001	96	4.00	0.05
4	4	0.1	0.001	96	4.00	0.1
5	4	0.5	0.001	96	3.98	0.5
6	4	1	0.001	96	3.96	0.99
7	4	2	0.001	96	3.92	1.96
8	6	0	0.001	94	6.00	0

components for the nominal 4 wt % PEO with varying NaCl concentrations (solutions #1–7). For this molecular weight of polymer, previous experiments used an optimal value of 6 wt % for TNE of PEO; hence, for comparison, components for a 6 wt % PEO solution are also shown.

2.2. Solution characterization

Zero shear viscosity of each polymer solution at 25 °C was determined using a stress-controlled rheometer (REOLOGICA Instruments AB, StressTech) utilizing a parallel plate geometry with a 45 mm diameter and a plate gap of 0.4 mm. Surface tension was measured using the du Noüy ring method by a surface tensiometer (Fisher Scientific, Model 21 Tensiomat). Solution conductivities were analyzed utilizing a portable waterproof conductivity meter with a plastic-bodied probe (Fisher Scientific, Accumet AP85). The presence of the salt increased the solution conductivity, while the solution viscosity and surface tension remained essentially unchanged over the range explored. Table 2 lists the measured properties for solutions #1–7 as the NaCl concentration is varied (see also Supplementary Information) and solution #8 for comparison.

2.3. Electrospinning

For the bowl edge electrospinning experiments, 78 ml of polymer solution was placed in an aluminum vessel having 9 cm inside diameter, 0.03 cm wall thickness, and 0.9 cm depth, as schematically depicted in Fig. 1. Along the bottom face of the vessel, the electrical connection of the bowl to the positive-polarity high voltage power supply (Glassman High Voltage, Model FC60R2) was secured by a bolt into blind tapped hole. When utilizing a highly-conductive polymer solution for bowl edge electrospinning, a single voltage level of 55 kV is used to both form the jets and fabricate the nanofibers, as detailed below.

At the bottom center of the bowl, a 1.27 cm diameter threaded hole was connected with a nylon hose-barb and poly vinyl tubing to two filled syringes, which were controlled via insulating wooden pushing rods by a pair of precision syringe pumps (New Era Systems, Model # NE-1000). The pumps (electrically-isolated from the two syringes) enabled continuous refilling of the polymer solution in the bowl at a user-specified rate, if desired. The grounded collector was a thin aluminum cylinder which encircled the bowl, having dimensions 39 cm in diameter, 0.01 cm in thickness, and 37 cm in height, thus providing a 15 cm working distance (defined as the distance in the radial direction between the outer edge of the bowl and the inner surface of the collector).

To maintain a constant relative humidity level (RH), an enclosure outside the collector volume but surrounding the experimental apparatus was fashioned out of plastic sheeting. A humidifier (Sunbeam, Model No. 696) using de-ionized water continuously provided air saturated with water vapor within the electrospinning volume while an exhaust hood above the apparatus created a slight vertical air flow in the region; RH was maintained between 35 and 40% as measured using a portable monitor (Fischer Scientific, Traceable). Under continuous refill at 700 μL/min (with an starting fill of 78 mL), 30 jets were initially generated (equally spaced around the bowl edge). Over the first 20 min of operation, the jet number slowly dropped (despite the constant level of fluid in the bowl) as small amounts of solid material accumulated on the bowl edge, blocking fiber-forming jets in these regions. As a result, the long-term stable jet number (measured for up to 2 h) was approximately 20 jets. Periodic cleaning of the bowl edge returned the jet number to 30; however, all long term experiments have an average jet number of 20 jets. Despite the "age" of the solution (time exposed to air or under the influence of the electric field), the jet number generated with a clean bowl edge was always ~30 jets which always decayed to ~20 jets as solid material accumulated. In all electrospinning experiments, conductive aluminum foil (Home 360™, 16 ± 1 μm thickness) was placed on the collector surface facing the source electrodes (needle or bowl) to gather the electrospun mat samples for additional analysis.

The polymer jets were illuminated by two sources: a halogen lamp (Northern Industrial Lighting, Model 1002) and a square array of white LEDs (Visual Instrumentation Corporation, Model 900445). A camcorder (Sony, Model DCR-SR68) and a digital single lens reflex (SLR) camera (Olympus, Model E-620) recorded movies and still images of the active electrospinning process as viewed from a top-looking down perspective. Post-processing video analysis enabled numbers of jets versus time to be determined.

For comparative TNE experiments, polymer solution was controllably-fed via a programmable syringe pump (New Era Systems, Model No. NE-1000) using a 10 mL plastic syringe with an attached 10 cm long stainless steel needle (gauge 20). The conductive needle was electrically connected to a positive-polarity power supply (Glassman High Voltage, Model No. FC60R2). A 15.25 cm diameter, aluminum collector plate was connected to ground potential and located a fixed working distance from the charged needle tip, centered on and oriented orthogonally to the needle's long axis.

Table 2
Comparison of solution properties with varying concentrations of salt.

Solution #	Properties		
	Zero shear viscosity (cP)	Conductivity (μS/cm)	Surface tension (mN/m)
1	1099 ± 55	85 ± 0.5	63.9 ± 0.9
2	1098 ± 55	237 ± 0.6	64.0 ± 0.4
3	1104 ± 55	885 ± 2.1	64.1 ± 0.4
4	1103 ± 55	1635 ± 4.0	63.7 ± 0.3
5	1045 ± 52	8257 ± 5.8	63.9 ± 0.1
6	1038 ± 52	15440 ± 17.3	64.0 ± 0.1
7	990 ± 50	30300 ± 100	63.2 ± 0.3
8	7477 ± 360	85 ± 0.2	59.6 ± 0.4

2.4. Fiber characterization

A scanning electron microscope (SEM) (Phenom FEI) operating at 5.0 kV was employed to analyze the nanofiber morphology within the electrospun mats. The mat samples were sputter-coated (Quoron Technologies, S67620) with Au–Pd at a thickness of ~100 Å in order to create a conductive surface and thereby reduce detrimental charging effects. The SEM images were analyzed to determine fiber characteristics using ImageJ Analyzer software where measurements of 25 distinct fibers were averaged to determine the mean diameter and standard deviation [87–92].

2.5. Fiber production rate and flow rate measurements

Nanofibrous material production rates (mass throughput or fabrication rates) were calculated by comparing the weight of the aluminum foil used to gather the sample before and after electrospinning for known time periods, measuring the resultant mat mass (PEO and salt), and then normalizing with time to obtain the fabrication rate in grams per hour (g/hr). A waiting period of 3 h in ambient conditions post-fiber fabrication was used to ensure that the mats were fully dried. By analyzing a contemporaneously-taken, top-viewing down video of the electrospinning process,

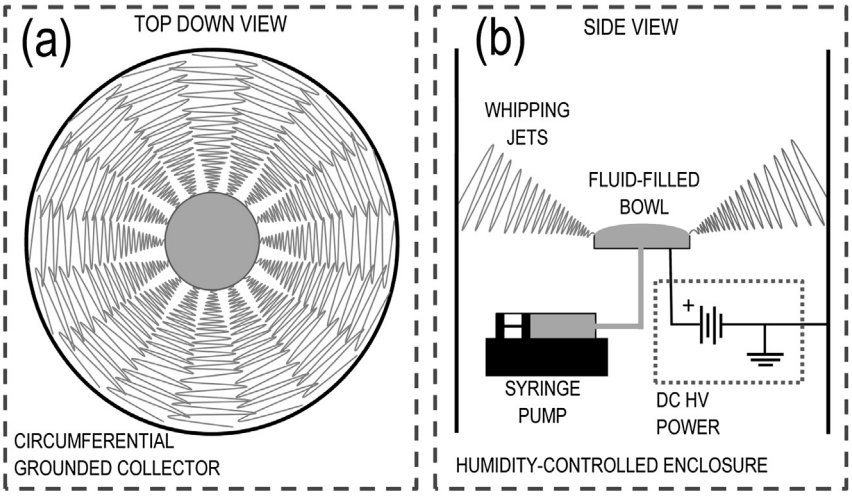

Fig. 1. Schematic diagram of the bowl edge electrospinning apparatus. (a) Top-looking down view of jets spinning directly from the bowl-lip to the collector. (b) A side view of the refill system and power supply.

the number of jets present during each minute of spinning can be measured and the production rate in grams per hour per jet determined. The flow rate per jet was calculated from the overall mass throughput per hour divided by the measured average number of jets over the collection period, and converted to an equivalent volumetric feed rate. Under streaming conditions (where fibers were not formed and instead solution was directly transferred to the collector) the fluid loss from the bowl over the initial 10 s time period of operation and the number of jets are measured, and the corresponding solution feed rates per jet (streaming loss rate) calculated.

2.6. Electric field simulations

Commercial software (Maxwell 3D, ANSOFT Corporation) modeled the electric field distribution generated within the bowl electrospinning geometry, where adaptive meshing and finite element methods are utilized to provide a converged solution. Optimized simulation parameters resulted in a minimum (maximum) mesh element dimension of <0.05 mm (0.13 mm) with a total ~10^6 mesh volume elements; in order to provide sufficient spatial resolution in the experimentally important regions, ~30% of the mesh volume elements defined the source electrode.

3. Results and discussion

3.1. Summary of solution properties

Electrospinning solutions of polyethylene oxide having a wide range of conductivities (solutions #1–7, Tables 1 and 2) were produced by adjusting the quantity of the inorganic salt additive sodium chloride. In principle, the addition of significant quantities of salt can alter the viscoelastic properties of the polymer solution, due to changes in solubility. As shown in Table 2 (see also Supplemental Information), the presence of the NaCl proportionally increased the solution conductivity, while the viscosity and surface tension values stayed approximately constant; hence, observed changes in electrospinning performance can be directly associated with the increase in available mobile charge carriers. In particular, Supplemental Fig. 2 presents viscosity versus shear rate over the range of shear from 0.1–1800 1/s for solutions #1, 4, and 7. No change in the viscoelastic response as a function of salt concentration is observed.

3.2. Mediation of feed rate via solution conductivity

In general, when electrospinning highly-conductive polymer solutions, the large number of available mobile charges inhibit or prevent the formation of stable fiber-forming jets [81]. Thus, it is often stated in reports discussing processing parameters for electrospinning that for a particular polymer above a certain additive concentration (a certain conductivity), the solution is no longer “spinnable” [81,86]. Such a potentially detrimental effect can be ameliorated to a certain extent by significantly increasing the applied voltage amplitude (and thereby, the electric field) [93]; thus we present experiments at high voltage levels (i.e., 55 kV, equivalent to an applied electric field of 1.03×10^7 V/m at the outside bowl edge for our experimental configuration). We note that no observable corona discharge was present during experiments.

With an applied voltage level fixed at 55 kV, jets formed on the rim of the source bowl for all solution types and either streamed fluid to (due to very high flow rate, Fig. 2a–c) or formed fibers (Fig. 2f) on the concentric collector. The jet formation process was similar to that reported for moderate conductivity solutions in a similar apparatus [50,51]. As summarized in Fig. 3 (filled circles), the average steady-state feed rate per jet is observed to decrease as the conductivity of the solution is increased, resulting in a dramatic transition from detrimental fluid streaming to nominal nanofiber-forming conditions. The shaded box indicates where streaming occurs and no fibers are formed whereas for the higher solution conductivities, nanofibers are produced. The overall trend of jet feed rate versus solution conductivity data is well-fit by a decaying exponential function (dark gray line) as: $y = A_1 e^{(-x/t_1)} + y_o$ where amplitude $A_1 = 394.8 \pm 53.6$ μL/min, $t_1 = 1076 \pm 162.2$ μS/cm, and the offset $y_o = 33.1 \pm 4.6$ μL/min.

Calculated flow rates (and the associated raw data) are shown in Table 3. For solutions #1–4 (having fluid conductivities in a range <2000 μS/cm) the flow rates are clearly too high for nanofiber formation: whereas most electrospinning processes have optimal feed rates of ~1–40 μL/min, these values are 10–100× greater. Even though the measured streaming loss rate drops by 3× over this range of increasing conductivity, the processing conditions are still

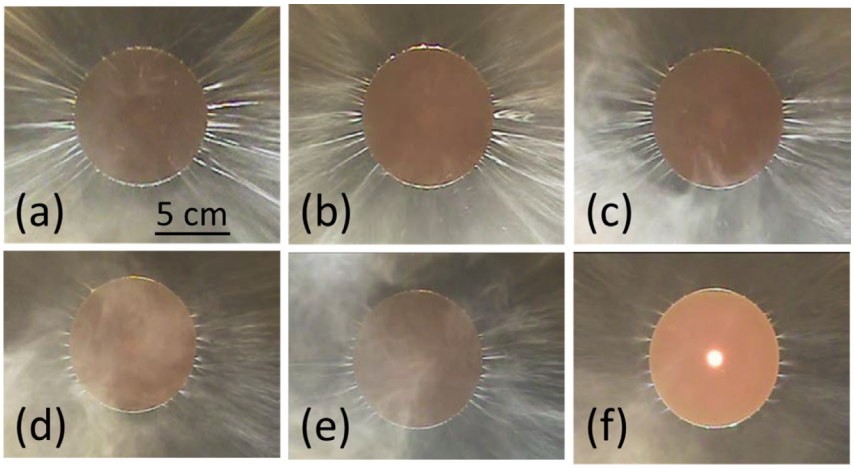

Fig. 2. Top–down view of bowl edge electrospinning for ~4 wt % PEO solutions with different salt concentration; solutions #2–7, (a)–(f). The transition from solely streaming/electrospraying events (a)–(c), to a mixture of streaming and fiber-forming jets (d)–(e), to finally only fiber-forming jets present (f) is seen, as both the jet number and solution feed rate are reduced. The size of the fluid jet is proportional to the reflectivity thus highly reflective, thick jets are associated with streaming. Notes: All images were taken 5 s after applying 55 kV. Lighting dominantly illuminates the horizontal direction in the image; jets are distributed relatively uniformly around the entire bowl edge.

not amenable for nanofiber formation. Streaming can be easily observed in the images of such experiments (Fig. 2a–c).

For solution #5–7, (having conductivities >8000 μS/cm), the average feed rate per jet is suppressed to the point that nanofibers are successfully fabricated at the high applied voltage level (55 kV). By visualizing the experiment for solutions #5 and #6 (Fig. 2d, e), a decrease in fluid streaming is observed as the conductivity increases and the feed rate is reduced. The electrospun mats from such solutions consist of regions with well-formed fibers alongside film-like morphology due to the solution streamed to the collector. For the highest conductivity fluid (solution #7; ~30,000 μS/cm), streaming is absent (Fig. 2f) and only fully-dried, high quality nanofibers are produced: hence, in this regime of operation, the solution's high conductivity results in a sufficiently low solution feed to enable uniform fabrication of quality nanofibers.

The resultant flow rates for solutions #5–7 (~30 μL/min) are consistent with the highest values normally utilized for TNE, which are generally associated with electrospinning polymer solutions containing particularly volatile solvents. More volatile solutions can be electrospun at higher feed rates because the solvent evaporates relatively quickly upon leaving the jet, resulting in both mass loss (thinning the fiber and thus accelerating the development of the whipping region) and solidification (which prevents the detrimental presence of solvent at the collector). Water (the solvent utilized in these experiments) has relatively low volatility and similar solutions of PEO generally require flow rate of <10 μL/min [49–51,53]. However, when electrospinning using high conductivity solutions, the presence of an extended whipping region (as visualized in Fig. 2f, and further discussed in Section 3.3) appears to enhance solvent loss and thus enables high quality fiber formation even at an elevated jet feed rate.

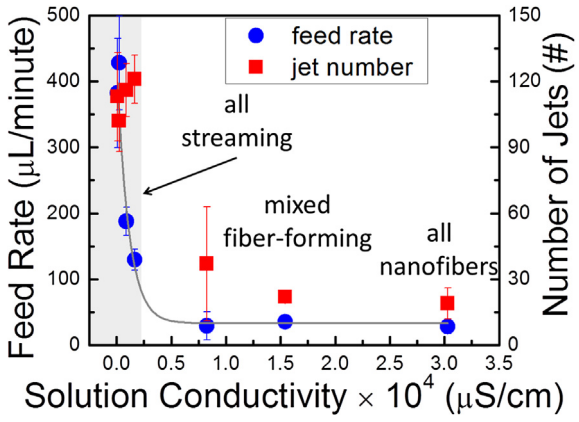

Fig. 3. Effect of the polymer solution conductivity on the jet number and average feed rate per jet. For lower conductivity, the high applied voltage causes streaming and no fiber formation (shaded gray area). The feed rate per jet decreases exponentially with fluid conductivity (blue circles, left axis). Overall, the jet number also reduces with higher conductivity solutions (red squares, right axis). (For interpretation of the references to color in this figure legend, the reader is referred to the web version of this article.)

Previous work on unconfined electrospinning and analysis of electric field-driven processes in general indicates that the feed rate through a jet can be estimated to scale as d^2E^2/η where E is the electric field, d the jet diameter and η the viscosity [51,52]. There is no indication of significant changes in η versus shear rate with salt concentration (see Supplementary Fig. 2); however changes in jet diameter will alter the fluid velocity (effective shear) and thus the pertinent viscosity. In Section 3.3 below, we argue that as the conductivity increases, changes in the electrostatic forces result in the coupled effect of smaller jet diameter and lower flow rate. Smaller diameter jets are more likely to experience whipping and changes in charge density on the proto-fiber (the stream of fluid past the jet (in the space between source and collector) which will ultimately become the fiber) due to changing conductivity will also facilitate formation of whipping.

Throughout this process, jets are robust and the quickly re-form (within 2–15 s) when they are accidentally extinguished (for instance by interaction with an existing fiber or another jet). Robust jets indicate that the electric field at the jet remains larger than a characteristic critical value (as discussed in Section 3.6). Thus a high density of jets can be maintained indefinitely while tuning the flow rate to a value appropriate for high quality fiber production. This approach is in sharp contrast to utilizing an overt reduction in the voltage level (and the associated electric field) to tune the flow rate (as utilized previously [50]), which has a secondary, deleterious effect of destabilizing jets and thus resulting in loss of jets with time.

3.3. Enhanced whipping region

As discussed above, Fig. 2 is composed of optical images of the unconfined electrospinning apparatus in operation at 55 kV on

Table 3
Streaming losses, mass throughput, number of jets, and feed rate per jet for ~4 wt % PEO solutions with an initial fluid fill of 78 mL, an applied voltage of 55 kV, and varying conductivities.

Solution #	Streaming loss (mL/10 s)	Mass throughput (g/hr)	Jet (#)	Feed rate (μL/min)
1	7.2 ± 0.9	–	113 ± 20	382.3 ± 82.8
2	7.3 ± 0.7	–	102 ± 14	428.0 ± 71.4
3	3.6 ± 0.2	–	116 ± 12	187.9 ± 21.0
4	2.6 ± 0.2	–	121 ± 11	129.3 ± 16.0
5	–	2.99 ± 0.68	37 ± 26	29.3 ± 21.4
6	–	2.39 ± 0.32	22 ± 3	35.3 ± 6.9
7	–	2.03 ± 0.04	19 ± 7	28.0 ± 10.3

solutions of varying conductivity. The decrease in feed rate is evident as the thick streams of fluid transition smoothly to much thinner (almost indistinguishable) fan-like projections from each jet site. Fig. 4c, d compares the process when electrospinning a moderate conductivity solution (solution #8) at 16 kV (using the hysteric method [50], initiation at 55 kV and reduced to 16 kV for operation) with that when exposing a very high conductivity solution (solution #7) to 55 kV. In examining Fig. 4c, ~31 jets are present and each jet possesses a distinct linear region followed by a whipping instability to thin and elongate the fiber, similar to what is commonly seen under a traditional needle electrospinning method. Note the general pattern of a clear linear region for 25–33% of the total working distance transitioning into a whipping region was independent of PEO solution concentration over the range of 4–7 wt %. The experimentally observed feed rate was 10.2 ± 2.5 μL/min for this 6 wt % PEO solution, and high quality fibers formed on the collector. (As discussed below, the 6 wt % moderate conductivity solution is utilized for some comparisons because of the presence of extensive beading when electrospinning the moderate conductivity 4 wt % PEO).

In contrast, Fig. 4d shows that for the 30 jets present using the highly-conductive, ~4 wt % PEO solution at a constant 55 kV, the whipping region begins almost directly at the bowl lip and extends entirely to the collector; the linear region (if present) is not discernible. The whipping region extends over the entire bowl-to-collector working distance, approximately 3× larger in relative dimension than usually observed in solution-phase electrospinning: furthermore, the volume encompassed by the whipping region fills virtually the entire vertical extent of the circumferential cylindrical collector with electrospun fibers. Hence even with the high individual jet fluid feed rate (28 μL/min compared to 10 μL/min in the moderate conductivity case), quality fibers are still formed over such an extended whipping distance.

Because the whipping process results from the inherent instability of a line of like charges (where perturbation from this linear arrangement results in forces that enhance that perturbation), the generation of the whipping region occurs when the fiber has sufficient charge density (which increases as the solvent evaporates

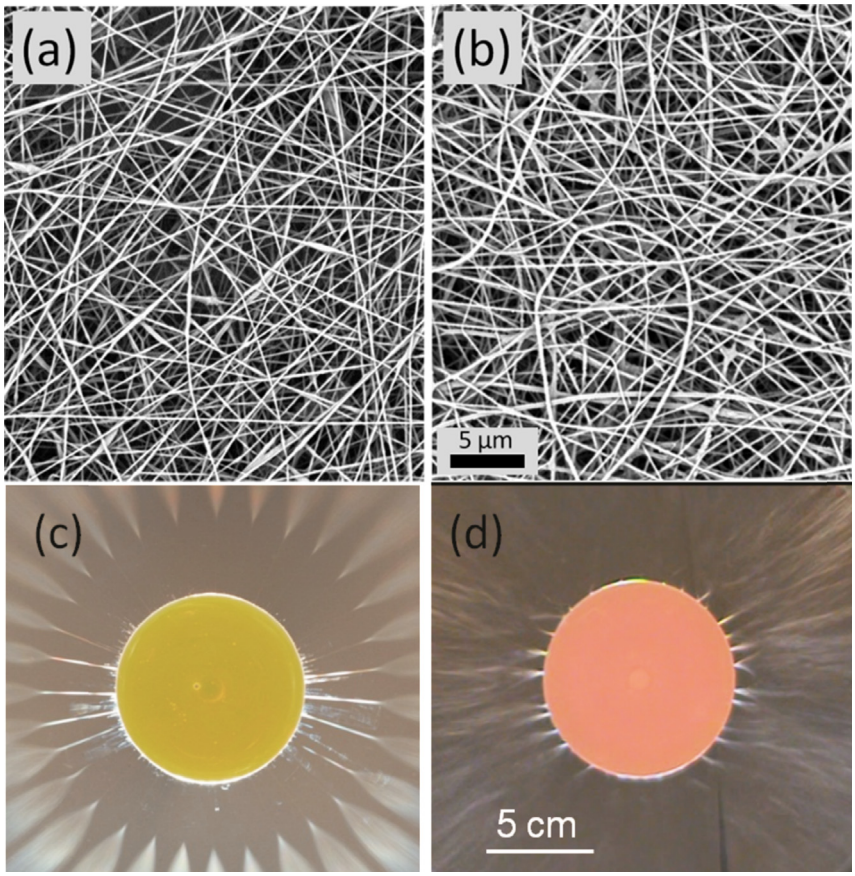

Fig. 4. Equivalent high quality nanofibers are produced by bowl-edge electrospinning in the hysteretic (a, c) or non-hysteretic regimes (b, d). For 6 wt % PEO solution with jets initiated at 55 kV then reduced to fiber-forming spinning at 16 kV (a) SEM image of mat showing fibers having diameters 200 ± 28 nm. For a nominal 4 wt % PEO with additional ~2 wt % NaCl continuously operated at 55 kV (b) SEM image of resultant mat showing fibers having diameters 193 ± 25 nm. (c) Top down view of 31 jets visible after 1 min of a 30 min hysteretic batch spinning process; clearly defined linear and whipping regions are visible; the throughput is ~40× that of TNE. (d) Top down view of 30 jets visible after 1 min of 120 min of non-hysteretic uninterrupted continuous spinning. The mass throughput is ~160× of TNE, using a polymer solution refill rate of 700 μL/min. No Taylor cone or linear region is observed; the whipping region appears to start directly at the lip of the bowl.

from the forming fiber) but is still sufficiently flexible to undergo bending. There have been many detailed treatments of the whipping region in traditional electrospinning [94–96]. Some general trends emerge: the larger the initial jet diameter, the smaller the surface area to volume, and thus, the slower the solvent evaporation process. In conjunction with this effect, thicker proto-fibers are more resistant to bending in general, and so generally due to both effects, thicker jets increase the length of the linear region. The other dominant effect on the whipping instability is the charge on the proto-fiber which is the drives the instability: both the applied voltage level and the fluid conductivity [97] are positively correlated with the surface charge density. Thus the total charge on the fluid surface in the high conductivity case is expected to be at least 3.4× larger (at 55 kV) than for a moderate conductivity fluid (at 16 kV). An overall increase in charge density raises the repulsive electrostatic forces that initiate whipping.

Although it is difficult to visualize the jet in high conductivity electrospinning and the presence of splaying to multiple jets at each site cannot be ruled out, the jet diameter in the high conductivity case appears to be smaller than that in the low conductivity scenario, even for a significant feed rate. Decrease in the jet diameter with increased conductivity is expected with one published theoretical treatment [98–100] predicting:

$$d \propto Q^{1/2} \kappa^{-1/6} \quad (1)$$

where d is the jet diameter, Q the flow rate, and κ the solution conductivity (with a co-factor on the order of $(\rho\varepsilon_0/\gamma)^{1/6}$, which here is constant, with ρ the solution density, ε_0 the permittivity of free space (or the full dielectric constant [98] in some treatments) and γ the surface tension.) Comparing the results from the solution with moderate conductivity electrospun at 15 kV (solution #1; $Q = 20.5$ μL/min [51] and $\kappa = 85$ μS/cm) with high conductivity fluid electrospun at 55 kV (solution #7; Q = 28 μL/min and κ = ~30,000 μS/cm), the high conductivity jet diameter is expected to be ~0.44 × smaller. (Note that here only 4 wt % PEO solutions are compared.) Based upon measurements of the cone-jet diameter (measured in the jet region at ~100 μm from the bowl edge) for solution #1 electrospun at 15 kV (with the corresponding feed rate above), the estimated jet diameter for the high conductivity case (at 55 kV) is <40 μm, which is much smaller than we have previously observed when electrospinning moderate conductivity PEO solutions.

In equation (1) there are two effects of increased κ: the reduced feed rate Q, as well as the direct $\kappa^{-1/6}$ dependence. Physically, the interaction between the applied electric field and the fluid simultaneously determines flow rate through the jet and the jet diameter, which are intimately connected: thus it is not the small diameter which creates the low flow rate nor the low flow rate which results in the small diameter, rather both effects are the result of the interaction between the applied field and the solution conductivity. This decrease in jet and proto-fiber diameter along with the increase in surface charge enhances the whipping instability. Overall, we conclude that increasing the solution conductivity alters the electrospinning process: creating a narrow diameter jet with a moderate feed rate and resulting in a long whipping region.

3.4. Fiber characterization and confirmation with different solution types

Scanning electron microscope images (Fig. 4b) confirm that narrow diameter nanofibers (193 ± 25 nm) are produced from the highly conductive solution #7 at 55 kV, with the resultant fibers comparable in size (200 ± 28 nm) with the nanofibers electrospun in the same system from solution #8 (moderate conductivity) under lower voltage conditions (16 kV). We note that the PEO concentration of solution #8 is 6 wt % whereas solutions #1–7 utilized in high conductivity/high voltage electrospinning are nominally 4 wt %. Fibers electrospun from the solution #1 (~4 wt %) under lower voltage conditions displayed an extensively beaded morphology preventing a clear comparison.

In order to further show the general applicability of this technique to a wider range of viscous solutions, a 6 wt % PEO with ~2 wt % NaCl (i.e., solution #8 + salt additive) was utilized for bowl electrospinning experiments (not shown). Even for such a highly viscous solution (viscosity ~6× the 4 wt % PEO solutions), jet initiation occurred rapidly, producing nanofibers having diameters 233 ± 52 nm, which overlaps the diameter observed from a salt-free solution at the same PEO concentration electrospun at low voltage (see above, 200 ± 28 nm).

3.5. Limits on cone-jet density

In unconfined electrospinning, the applied voltage determines the ability to form fluid perturbations (i.e., the time scale over which perturbations will spontaneously form) and the minimum spacing between cone-jet (perturbation) sites, here defined as λ, and thus the maximum possible jet density [51,52]. As detailed in previous works, at relatively low electric field strengths, the interactions between surface tension and the applied field sets the limit on λ; however at higher field strengths (high applied voltages where the surface charge density and flow rates are high) and/or when cone-jets are large due to high viscosity and/or flow rate, jet-to-jet interactions can be important and limit jet density [52]. Essentially, each cone-jet is charged and the repulsive force from neighboring jets can compress and prevent forming perturbations, limiting jet density.

In Fig. 3 and Table 2, the observed jet number at 55 kV as a function of solution conductivity is presented. At the lowest conductivity (solutions #1–4), the experimentally observed number of jets increases slightly with conductivity and is approximately 100–125. The observed slight increase in jet number (Fig. 3) with increasing conductivity and decreasing flow rate (and jet diameter) indicates that inter-jet interactions are significant. If the jet number was determined by surface tension effects alone, the electric field of 1.03×10^7 V/m at 55 kV results in a prediction of $\lambda = 2\pi\ (1.5\gamma/\varepsilon_0 E^2) = 0.6$ mm (where γ is the surface tension, 64 mN/m, E is the electric field, and ε_0 is the permittivity of free space) [51], or ~450 jets (over the circumference of the bowl), which is about 4× the experimentally observed values for moderate conductivity solutions. As the conductivity increases (solutions #5–7) and the whipping instability is formed at the bowl edge, the jet number further drops with a maximum jet number of 20–30 jets (as discussed further in Sections 2.4 and 3.6). Thus, although the specific mechanism(s) are unclear, throughout this range of conductivity, the jet number is set by inter-jet interactions. Based on previous work, inter-jet interactions generally result from repulsive electrostatic interactions, which will increase with charge density and thus are dependent on both applied voltage and (more weakly) solution conductivity.

Hence, the large applied voltage has the advantages of ensuring robust jets, allowing electrospinning from high conductivity solutions, and increasing the whipping region length (under high conductivity); however, these same advantages likely result in inter-jet interactions which limit jet number. As discussed in Section 3.6, despite the relatively large area per jet (jet-to-jet spacing of ~1.4 cm), the higher throughput per jet (enabled by the extended whipping region) and the indefinite jet persistence results in an overall significant gain in fiber production when electrospinning in

this manner. In particular utilizing the bowl apparatus for moderate conductivity solutions at 16 kV (Fig. 4a, c) results in a production rate of 40× that of a single needle [50]. Here the maximum jet number is ~32 and jet number decays slowly with time over the length of a 20 min experiment. Utilizing the same bowl to electrospin a high conductivity solution at 55 kV (Fig. 4b, d) results in a production rate of 125× that of a single needle (see Section 3.6). Even with fewer jets at beginning of the experiment, the higher throughput per jet and the absence of jet loss results in an overall gain in production.

3.6. Jet stability and fiber production rate

Fig. 5 illustrates the long term stability of jet number for the ultra-conductive solution #7 at a fixed applied voltage level of 55 kV under continuous feed (700 μL/min, see Section 2.3). As discussed in greater detail in Section 2.3, an inadvertent consequence of the high mass throughput of this process is that the bowl lip becomes contaminated with solid fibrous material. This contamination statistically reduces the average jet number to ~20. However, these 20 jets are then indefinitely robust at the given fill rate where polymer solution in the bowl is replenished to offset the fluid loss due to nanofiber formation: thus electrospinning will continue indefinitely. In contrast with previous work in unconfined systems where different voltage levels/fields were required to tune feed rate to an appropriate value for high quality fiber formation, utilizing the solution conductivity to tune feed rate has the added advantage that the jets are permanently present and can be regenerated (if needed) at this voltage/electric field level.

The presence of indefinitely robust jets is indicative that the effective electric field at the jet is greater than some critical value. In the sub-critical regime, an applied electric field will result in fluid perturbations which grow and then saturate and become static [101]. Above a critical electric field value, similar fluid perturbations are unstable and transition into jets. For most fluids the field needed to maintain a jet is significantly smaller (between 0.5 and 0.1×) the field needed to form jets. Such "hysteretic" jets (produced under a high voltage and maintained at a lower voltage value) are quasi-stable but are randomly, spontaneously extinguished with time. Once a hysteretic jet is extinguished (for instance by fluctuation or a momentary contact with an existing fiber or another jet) it will not spontaneously re-form. In the experiments described here, the applied voltage clearly leads to an electric field which is above the critical electric field needed for jet formation. Not only is the jet number stable with time, when on occasion, jets are randomly extinguished, a new jet is formed immediately (within 2–15 s).

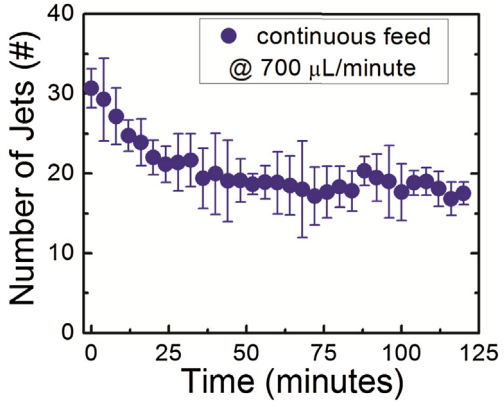

Fig. 5. Number of spinning sites at the bowl edge versus time when using a highly-conductive fluid (solution #7). The applied voltage is fixed at 55 kV and the bowl is being continuously refilled at a 700 μL/min rate.

Analytical predictions of the critical electric field to form a jet from a droplet of radius a are generally of the form [102] $E_{critical} \sim N(\gamma/\varepsilon_0 a)^{1/2}$ where N is a constant on the order of 1. For unconfined systems, such as in use here, there is no characteristic droplet size. Previous workers have proposed the capillarity length (a characteristic length that, for instance, determines the size of the meniscus when a fluid encounters a vertical wall [103]) given by $a = (\gamma/\rho g)^{1/2}$ as the appropriate length scale in an unconfined system [42]. However, gravity plays no role in this unconfined configuration and we have previously argued that the characteristic length scales in such a viscous system are much smaller than the capillarity length (which for this solution is ~2.5 mm) [52]. Experimentally we find that for moderate conductivity solutions, the critical applied voltage (for this bowl configuration) is 30–45 kV or an electric field range of 5.6–8.4 × 10^6 V/m, which would be consistent with a characteristic length of ~100–200 μm. Previously [50] we argued that radius of observed fluid perturbations in this system (with solution #1) was~ 200 μm which is consistent with these critical values. As the characteristic length decreases (to as low as 40 μm) with high conductivity, the electric field expected for 55 kV (1.0 × 10^7 V/m) is still similar to or above E_c.

Fabricating nanofibers with a relatively high average feed rate per jet from approximately 20 simultaneous stable spinning sites results in a ~2 g/hr experimentally measured mass throughput; such a production rate corresponds to ~125× greater than TNE typically provides. The high production rate is due to the combined beneficial effects of multiple parallel jets (~20–30) and a relatively high feed rate per jet compared with the TNE case (~3–4×).

4. Conclusion

In this work, the flow rate through a spontaneously formed jet was controlled (by over an order of magnitude) by solely adjusting the solution conductivity. Increasing solution conductivity led to a narrower jet and a reduced flow rate. The very narrow jet and enhanced surface charge density facilitated formation of a very long whipping region (with essentially no linear region), which enabled high quality fiber formation. Jets were present indefinitely and produced high quality fibers at a relatively high throughput per jet due to the extended whipping region. Successful fiber formation from such a highly conductive solution reveals new potential pathways to fabricate highly conductive nanofibers and allows exploration of a novel processing regime where feed rate is controlled by solution parameters. Although here a permanent salt compound was utilized, use of transient ionic charges [75] would enable application of this approach without inclusion of a salt or charged compound in the final nanofiber; thus producing low conductivity nanofibers while utilizing the innate effects of a high conductivity solution. Alternatively, for polymers such as polyethylene oxide which can be successfully cross-linked with ultraviolet light [104,105], the resulting nanofibers could be swollen in water to remove excess salt after fabrication.

Acknowledgments

This work was supported by NSF CMMI-0800237. The authors thank Hai Bui and Dzung Nguyen for fabrication of the bowl electrospinning apparatus; Judy Elson for assistance on the SEM measurements; Wendy Krause, Julie Willoughby, and Xiangwu Zhang for use of instrumentation to characterize polymer solution properties.

Appendix A. Supplementary data

Supplementary data related to this article can be found inline at http://dx.doi.org/10.1016/j.polymer.2014.10.007.

References

[1] Huang ZM, Zhang YZ, Kotaki M, Ramakrishna S. Compos Sci Technol 2003;63(15):2223–53.
[2] Liu HQ, Kameoka J, Czaplewski DA, Craighead HG. Nano Lett 2004;4(4):671–5.
[3] Wang XY, Drew C, Lee SH, Senecal KJ, Kumar J, Sarnuelson LA. Nano Lett 2002;2(11):1273–5.
[4] Scampicchio M, Bulbarello A, Arecchi A, Cosio MS, Benedetti S, Mannino S. Electroanal 2012;24(4):719–25.
[5] McCullen SD, Ramaswamy S, Clarke LI, Gorga RE. Wiley Interdiscip Rev Nanomedicine Nanobiotechnol 2009;1(4):369–90.
[6] Pham QP, Sharma U, Mikos AG. Tissue Eng 2006;12(5):1197–211.
[7] Greiner A, Wendorff JH. Angew Chem Int Ed 2007;46(30):5670–703.
[8] Zhong SP, Zhang YZ, Lim CT. Wiley Interdiscip Rev Nanomedicine Nanobiotechnol 2010;2(5):510–25.
[9] Liang D, Hsiao BS, Chu B. Adv Drug Deliv Rev 2007;59(14):1392–412.
[10] Sill TJ, von Recum HA. Biomaterials 2008;29(13):1989–2006.
[11] Agarwal S, Wendorff JH, Greiner A. Polymer 2008;49(26):5603–21.
[12] Barhate RS, Ramakrishna S. J Membr Sci 2007;296(1–2):1–8.
[13] Chigome S, Darko G, Torto N. Analyst 2011;136(14):2879–89.
[14] Thavasi V, Singh G, Ramakrishna S. Energy Environ Sci 2008;1(2):205–21.
[15] Cavaliere S, Subianto S, Savych I, Jones DJ, Roziere J. Energy Environ Sci 2011;4(12):4761–85.
[16] Dong ZX, Kennedy SJ, Wu YQ. J Power Sources 2011;196(11):4886–904.
[17] Zhang XW, Ji LW, Toprakci O, Liang YZ, Alcoutlabi M. Polym Rev 2011;51(3):239–64.
[18] Mao XW, Hatton TA, Rutledge GC. Curr Org Chem 2013;17(13):1390–401.
[19] Burger C, Hsiao BS, Chu B. Nanofibrous materials and their applications. Annual review of materials research, vol. 36. Palo Alto: Annual Reviews; 2006. p. 333–68.
[20] Sarkar K, Gomez C, Zambrano S, Ramirez M, de Hoyos E, Vasquez H, et al. Mater Today 2010;13(11):12–4.
[21] Weitz RT, Harnau L, Rauschenbach S, Burghard M, Kern K. Nano Lett 2008;8(4):1187–91.
[22] Luo CJ, Stoyanov SD, Stride E, Pelan E, Edirisinghe M. Chem Soc Rev 2012;41(13):4708–35.
[23] Sun ZC, Zussman E, Yarin AL, Wendorff JH, Greiner A. Adv Mater 2003;15(22):1929–32.
[24] Yarin AL. Polym Adv Technol 2011;22(3):310–7.
[25] Yang JM, Yu DG. J Polym Res 2012;19(2).
[26] Yu DG, Lu P, Branford-White C, Yang JH, Wang X. Nanotechnology 2011;22(43).
[27] Yu DG, White K, Yang JH, Wang X, Qian W, Li Y. Mater Lett 2012;67(1):78–80.
[28] Sinha-Ray S, Yarin AL, Pourdeyhimi B. Carbon 2010;48(12):3575–8.
[29] Sinha-Ray S, Zhang Y, Yarin AL, Davis SC, Pourdeyhimi B. Biomacromolecules 2011;12(6):2357–63.
[30] Dosunmu OO, Chase GG, Kataphinan W, Reneker DH. Nanotechnology 2006;17(4):1123–7.
[31] Varabhas JS, Chase GG, Reneker DH. Polymer 2008;49(19):4226–9.
[32] Angammana CJ, Jayaram SH. IEEE Trans Ind Appl 2011;47(2):1028–35.
[33] Bowman J, Taylor M, Sharma V, Lynch A, Chadha S. Multispinneret methodologies for high throughput electrospun nanofiber. In: Burganos VN, Noble RD, Asaeda M, Ayral A, LeRoux JD, editors. Membranes-preparation, properties and applications, vol. 752. Warrendale: Materials Research Society; 2003. p. 15–9.
[34] Kim G, Cho YS, Kim WD. Eur Polym J 2006;42(9):2031–8.
[35] Tomaszewski W, Szadkowski M. Fibres Text East Eur 2005;13(4):22–6.
[36] Theron SA, Yarin AL, Zussman E, Kroll E. Polymer 2005;46(9):2889–99.
[37] Yang Y, Jia ZD, Li Q, Hou L, Gao HF, Wang LM, et al. Multiple jets in electrospinning. New York: IEEE; 2006.
[38] Zhou FL, Gong RH, Porat I. J Mater Sci 2009;44(20):5501–8.
[39] Chase GG, Varabhas JS, Reneker DH. J Eng Fibers Fabr 2011;6(3):32–8.
[40] Niu HT, Lin T. J Nanomater 2012:13.
[41] Yarin AL, Zussman E. Polymer 2004;45(9):2977–80.
[42] Lukas D, Sarkar A, Pokorny P. J Appl Phys 2008;103(8).
[43] Cengiz F, Dao TA, Jirsak O. Polym Eng Sci 2010;50(5):936–43.
[44] Cengiz F, Jirsak O. Fibers Polym 2009;10(2):177–84.
[45] Yener F, Jirsak O. J Nanomater 2012. 839317.
[46] Niu HT, Lin T, Wang XG. J Appl Polym Sci 2009;114(6):3524–30.
[47] Niu HT, Wang XG, Lin T. J Text Inst 2012;103(7):787–94.
[48] Forward KM, Flores A, Rutledge GC. Chem Eng Sci 2013;104:250–9.
[49] Thoppey NM, Bochinski JR, Clarke LI, Gorga RE. Polymer 2010;51(21):4928–36.
[50] Thoppey NM, Bochinski JR, Clarke LI, Gorga RE. Nanotechnology 2011;22(34):345301.
[51] Thoppey NM, Gorga RE, Bochinski JR, Clarke LI. Macromolecules 2012;45:6527.
[52] Roman MP, Thoppey NM, Gorga RE, Bochinski JR, Clarke LI. Macromolecules 2013;46:7352–62.
[53] Thoppey NM. Edge electrospinning for high throughput production of nanofibers. Fiber and polymer science. PhD thesis. Raleigh: North Carolina State University; 2012. p. 177.
[54] Theron SA, Zussman E, Yarin AL. Polymer 2004;45(6):2017–30.
[55] Demir MM, Yilgor I, Yilgor E, Erman B. Polymer 2002;43(11):3303–9.
[56] Tan SH, Inai R, Kotaki M, Ramakrishna S. Polymer 2005;46(16):6128–34.
[57] Choi JS, Lee SW, Jeong L, Bae SH, Min BC, Youk JH, et al. Int J Biol Macromol 2004;34(4):249–56.
[58] Dong H, Nyame V, Macdiarmid AG, Jones WE. J Polym Sci Part B-Polym Phys 2004;42(21):3934–42.
[59] Son WK, Youk JH, Lee TS, Park WH. Polymer 2004;45(9):2959–66.
[60] Zong XH, Kim K, Fang DF, Ran SF, Hsiao BS, Chu B. Polymer 2002;43(16):4403–12.
[61] Arayanarakul K, Choktaweesap N, Aht-ong D, Meechaisue C, Supaphol P. Macromol Mater Eng 2006;291(6):581–91.
[62] Du JM, Zhang XW. J Appl Polym Sci 2008;109(5):2935–41.
[63] Fallahi D, Rafizadeh M, Mohammadi N, Vahidi B. E-Polymers 2008:10.
[64] Kim SJ, Lee CK, Kim SI. J Appl Polym Sci 2005;96(4):1388–93.
[65] Mit-uppatham C, Nithitanakul M, Supaphol P. Macromol Chem Phys 2004;205(17):2327–38.
[66] Qin XH, Yang EL, Li N, Wang SY. J Appl Polym Sci 2007;103(6):3865–70.
[67] Barakat NAM, Kanjwal MA, Sheikh FA, Kim HY. Polymer 2009;50(18):4389–96.
[68] Cooper A, Bhattarai N, Kievit FM, Rossol M, Zhang MQ. Phys Chem Chem Phys 2011;13(21):9969–72.
[69] Gupta A, Saquing CD, Afshari M, Tonelli AE, Khan SA, Kotek R. Macromolecules 2009;42(3):709–15.
[70] Heikkila P, Harlin A. Eur Polym J 2008;44(10):3067–79.
[71] Heikkila P, Harlin A. Express Polym Lett 2009;3(7):437–45.
[72] Jacobs V, Anandjiwala RD, Maaza M. J Appl Polym Sci 2010;115(5):3130–6.
[73] Li N, Qin XH, Lin L, Wang SY. Polym Eng Sci 2008;48(12):2362–6.
[74] Lin Z, Woodroof MD, Ji LW, Liang YZ, Krause W, Zhang XW. J Appl Polym Sci 2010;116(2):895–901.
[75] Moghe AK, Hufenus R, Hudson SM, Gupta BS. Polymer 2009;50(14):3311–8.
[76] Moon S, Choi J, Farris RJ. Polym Eng Sci 2011;51(6):1122–9.
[77] Su P, Wang CJ, Yang XY, Chen XY, Gao CY, Feng XX, et al. Carbohydr Polym 2011;84(1):239–46.
[78] Tong HW, Wang M. J Appl Polym Sci 2011;120(3):1694–706.
[79] Song BT, Cui WG, Chang J. J Appl Polym Sci 2011;122(2):1047–52.
[80] Zhang QC, Wang LH, Wei ZM, Wang XJ, Long SR, Yang J. J Polym Sci Part B Polym Phys 2012;50(14):1004–12.
[81] Angammana CJ, Jayaram SH. IEEE Trans Ind Appl 2011;47(3):1109–17.
[82] Xin Y, Reneker DH. Polymer 2012;53(16):3629–35.
[83] Fong H, Chun I, Reneker DH. Polymer 1999;40(16):4585–92.
[84] Wang YZ, Wang BC, Wang GX, Yin TY, Yu QS. Polym Bull 2009;63(2):259–65.
[85] Zhang QC, Li MX, Liu J, Long SR, Yang J, Wang XJ. Colloid Polym Sci 2012;290(9):793–9.
[86] Morota K, Matsumoto H, Mizukoshi T, Konosu Y, Minagawa M, Tanioka A, et al. J Colloid Interface Sci 2004;279(2):484–92.
[87] Maity S, Downen LN, Bochinski JR, Clarke LI. Polymer 2011;52(7):1674–85.
[88] McCullen SD, Stano KL, Stevens DR, Roberts WA, Monteiro-Riviere NA, Clarke LI, et al. J Appl Polym Sci 2007;105(3):1668–78.
[89] McCullen SD, Stevens DR, Roberts WA, Clarke LI, Bernacki SH, Gorga RE, et al. Int J Nanomedicine 2007;2(2):253–63.
[90] McCullen SD, Stevens DR, Roberts WA, Ojha SS, Clarke LI, Gorga RE. Macromolecules 2007;40(4):997–1003.
[91] Ojha SS, Stevens DR, Hoffman TJ, Stano K, Klossner R, Scott MC, et al. Biomacromolecules 2008;9(9):2523–9.
[92] Ojha SS, Stevens DR, Stano K, Hoffman T, Clarke LI, Gorga RE. Macromolecules 2008;41(7):2509–13.
[93] Wang C, Cheng YW, Hsu CH, Chien HS, Tsou SY. J Polym Res 2011;18(1):111–23.
[94] Reneker DH, Yarin AL, Fong H, Koombhongse S. J Appl Phys 2000;87(9):4531–47.
[95] Yarin AL, Koombhongse S, Reneker DH. J Appl Phys 2001;89(5):3018–26.
[96] Reneker DH, Yarin AL, Zussman E, Xu H. Electrospinning of nanofibers from polymer solutions and melts. In: Aref H, VanDerGiessen E, editors. Advances in applied mechanics, 41. San Diego: Elsevier Academic Press Inc; 2007. p. 43–195.
[97] Bhattacharjee PK, Schneider TM, Brenner MP, McKinley GH, Rutledge GC. J Appl Phys 2010;107(4):044306.
[98] Ganan-Calvo AM. Phys Rev Lett 1997;79(2):217–20.
[99] Gamero-Castano M. J Fluid Mech 2010;662:493–513.
[100] Maisser A, Attoui MB, Ganan-Calvo AM, Szymanski WW. J Nanopart Res 2013;15(1):1318.
[101] Reznik SN, Yarin AL, Theron A, Zussman E. J Fluid Mech 2004;516:349–77.
[102] Higuera FJ. Phys Rev E 2008;78(1):11.
[103] de Gennes P-G, Brochard-Wyart F, Quere D. Capillarity and wetting phenomena. New York: Springer; 2010.
[104] Zhou CJ, Wang QW, Wu QL. Carbohydr Polym 2012;87(2):1779–86.
[105] Doytcheva M, Stamenova R, Zvetkov V, Tsvetanov CB. Polymer 1998;39(26):6715–21.